JOURNAL OF COMPUTATIONAL PHYSICS 52, 142–162 (1983)

# Computing Variational Bounds for Flow through Random Aggregates of Spheres*

JAMES G. BERRYMAN

*Lawrence Livermore National Laboratory, P. O. Box 808, L-200, Livermore, California 94550*

Received November 16, 1982

Known formulas for variational bounds on Darcy's constant for slow flow through porous media depend on two-point and three-point spatial correlation functions. Certain bounds due to Prager and Doi depending only a two-point correlation functions have been calculated for the first time for random aggregates of spheres with packing fractions ($\eta$) up to $\eta = 0.64$. Three radial distribution functions for hard spheres were tested for $\eta$ up to 0.49: (1) the uniform distribution or "well-stirred approximation," (2) the Percus–Yevick approximation, and (3) the semi-empirical distribution of Verlet and Weis. The empirical radial distribution functions of Bennett and Finney were used for packing fractions near the random-close-packing limit ($\eta_{RCP} \sim 0.64$). An accurate multidimensional Monte Carlo integration method (VEGAS) developed by Lepage was used to compute the required two-point correlation functions. The results show that Doi's bounds are preferred for $\eta < 0.10$ while Prager's bounds are preferred for $\eta > 0.10$. The "upper bounds" computed using the well-stirred approximation actually become negative (which is physically impossible) as $\eta$ increases, indicating the very limited value of this approximation. The other two choices of radial distribution function give reasonable results for $\eta$ up to 0.49. However, these bounds do not decrease with $\eta$ as fast as expected for large $\eta$. It is concluded that variational bounds dependent on three-point correlation functions are required to obtain more accurate bounds on Darcy's constant for large $\eta$.

## 1. INTRODUCTION

When gravitational effects are neglected, Darcy's law [1] for slow flow through porous media states that the average discharge per unit of cross-sectional area normal to the direction of flow ($Q$ in units of velocity) is proportional to the negative





0021-9991/83 $3.00

gradient of pressure and inversely proportional to the shear viscosity of the fluid ($\mu$), i.e.,

$$\mathbf{Q} = -\frac{k}{\mu}\nabla P. \tag{1}$$

The proportionality constant $k$ is known as Darcy's constant or alternatively as the fluid permeability of the porous medium. The permeability is a complicated function of the statistical geometry for random porous materials. In certain idealized cases with either periodic [2] or random [3–5] arrays of spheres at very small concentrations of solid particles, asymptotic expansions for the permeability as a function of packing fraction (volume concentration) $\eta$ are available. Only recently have methods been developed to calculate $k$ for periodic arrays of spheres at large values of $\eta$ [6, 7].

In most cases of practical interest, useful theoretical estimates of the permeability are not yet available so empirical formulas (based on dimensional analysis) such as the Kozeny–Carman equations are used [8]. General variational bounds have been developed by Prager [9] and Doi [10]. However, these formulas involve two-point or three-point spatial correlation functions which are not generally known for real porous materials. Therefore, these bounds have only been evaluated for artificial models or for limiting cases of small concentrations of spherical particles.

The purpose of the present paper is to develop the numerical methods required to evaluate these formulas for random aggregates of spherical particles for packing fractions up to and including the theoretical maximum at random close packing ($\eta_{RCP} \sim 0.64$.). The major difficulty with this enterprise is the calculation of the two-point and three-point correlation functions which appear in the formulas. We restrict discussion to those variational bounds depending only on two-point correlation functions since these functions can now be calculated with an accuracy of a few percent for random aggregates of spheres. These calculations were made possible partially by the extensive published literature on radial distribution functions for hard-sphere fluids [11–13], partially by the recent development of an accurate multidimensional, adaptive Monte Carlo integration method which works well even for poorly behaved integrands such as the pair distribution function [14], and partially by the techniques developed in the present work.

In Section 2, the upper bounds on permeability are presented and the numerical problem to be solved is formulated. An analytical example using the well-stirred approximation to the radial distribution function is presented in Section 3. This analytical example is interesting in its own right but it also plays two essential roles in the subsequent analysis: (1) The example provides a nontrivial check on the Monte Carlo integration routine. (2) These results also serve as a leading contribution to the more realistic calculations in Section 4. Two approximations to the radial distribution function are treated in Section 4. Exact analytical results are known [15, 16] for the Percus–Yevick approximation to the hard-sphere radial distribution function, so this approximation is fairly convenient. The semi-empirical formulas of Verlet and Weis

[11] for the radial distribution function agree (±3 %) with Monte Carlo results on hard spheres up to packing fractions of about 0.49 and are not much more difficult to implement numerically than the Percus–Yevick approximation [17]. Section 4 also summarizes the results for the bounds on permeability obtained using these two approximations and compares the results to empirical formulas and exact results on other related systems of particles.

## 2. Bounds on Permeability

Prager [9] and Doi [10] have presented variational methods which lead to upper bounds on the permeability of general porous media if certain spatial correlation functions are known. Doi's paper contains one bound on permeability which depends on three distinct two-point correlation functions. Prager's paper contains several formulas, some of which depend on three-point correlation functions. Since the three-point correlation functions cannot yet be calculated as accurately as the two-point correlation functions for any model material, our discussion will be restricted to formulas depending only on two-point correlation functions.

Using Doi's notation, the bounds to be considered are Prager's simplified upper bound

$$k_P = \frac{9}{10}\int_0^\infty d\zeta\zeta[F_{vv}(\zeta) - \phi^2]/(1-\phi)^2 \tag{2}$$

and Doi's upper bound

$$k_D = \frac{2}{3}\int_0^\infty d\zeta\zeta\left[F_{vv}(\zeta) - \frac{2\phi}{s}F_{sv}(\zeta) + \frac{\phi^2}{s^2}F_{ss}(\zeta)\right]. \tag{3}$$

In Eqs. (2) and (3), $\phi$ is the porosity (void space per unit volume) and $s$ is the specific surface area (pore surface area per unit volume). The correlation functions are defined in terms of a function $f(\mathbf{r})$ which takes the value unity in the void and the value zero in the solid. Then the correlation functions are defined by the equations

$$F_{vv}(\boldsymbol{\zeta}) = \langle f(\mathbf{r})\, f(\mathbf{r}+\boldsymbol{\zeta})\rangle \tag{4}$$

$$F_{sv}(\boldsymbol{\zeta}) = \langle |\nabla f(\mathbf{r})|\, f(\mathbf{r}+\boldsymbol{\zeta})\rangle \tag{5}$$

$$F_{ss}(\boldsymbol{\zeta}) = \langle |\nabla f(\mathbf{r})|\, |\nabla f(\mathbf{r}+\boldsymbol{\zeta})|\rangle \tag{6}$$

where the brackets indicate a volume average over the spatial coordinate $\mathbf{r}$. These functions are called void–void, surface–void, and surface–surface correlation functions. For the macroscopically isotropic materials considered here, all three functions depend only on $\zeta = |\boldsymbol{\zeta}|$. As $\zeta \to \infty$, these functions have the limiting forms

$$F_{vv}(\zeta) \to \phi^2, \qquad F_{sv}(\zeta) \to s\phi, \qquad F_{ss}(\zeta) \to s^2. \tag{7}$$

As $\zeta \to 0$, Prager notes that

$$F_{vv}(\zeta) \to \phi \qquad \text{and} \qquad \frac{dF_{vv}(\zeta)}{d\zeta} \to -\frac{s}{4}. \tag{8}$$

So far these formulas are completely general and could be applied to any macroscopically isotropic porous material for which the correlation functions were known. For particular porous materials, these correlation functions can be measured by careful examination of photographs of cross sections of the material [18]. Lacking this information, we choose to study a random aggregate of hard spheres with uniform radii. This model is convenient because a vast literature exists on the statistical properties of the hard sphere model of fluids [19] and also because such a model can readily be built in the laboratory [13, 20].

For any particular configuration of spheres (each with diameter $\sigma$), the function $f(\mathbf{r})$ can be written (following Doi) as

$$f(\mathbf{r}) = h(\mathbf{r}; R) = \prod_n \theta(|\mathbf{r} - \mathbf{r}_n| - R) \tag{9}$$

where

$$\begin{aligned} \theta(x) &= 1 \qquad x \geqslant 0 \\ &= 0 \qquad x < 0 \end{aligned} \tag{10}$$

and $\mathbf{r}_n$ denotes the center of the $n$th sphere and $R = \sigma/2$. Then it follows from (9) that

$$|\nabla f(\mathbf{r})| = \frac{\partial}{\partial R} h(\mathbf{r}; R). \tag{11}$$

Defining

$$H(\boldsymbol{\zeta}; x, y) = \langle h(\mathbf{r}; x)\, h(\mathbf{r} + \boldsymbol{\zeta}; y) \rangle, \tag{12}$$

we find that

$$F_{vv}(\boldsymbol{\zeta}) = H(\boldsymbol{\zeta}; R, R) \tag{13}$$

$$F_{sv}(\boldsymbol{\zeta}) = \frac{\partial}{\partial x} H((\boldsymbol{\zeta}; x, y)|_{x=y=R} \tag{14}$$

and

$$F_{ss}(\boldsymbol{\zeta}) = \frac{\partial^2}{\partial x\, \partial y} H(\boldsymbol{\zeta}; x, y)|_{x=y=R}. \tag{15}$$

Thus, all three two-point correlation functions are completely determined by the generating function $H(\boldsymbol{\zeta}; x, y)$.

The general form of the generating function (12) can be found by slightly modifying an argument used by Weissberg and Prager [21] to evaluate $H(\zeta; R, R)$. Let $\rho$ be the number of spheres per unit volume and $\eta = \pi\sigma^3\rho/6 = 1 - \phi$ be the packing fraction. Define the radial (pair) distribution function $g(r)$ so that, if a particle is located at the origin, the expected number of particle centers to be found in the spherical shell between $r$ and $r + dr$ is $4\pi r^2 \rho g(r)\, dr$. Now $H(\zeta; x, y)$ is the probability that two points of the porous medium $\mathbf{r}$ and $\mathbf{r} + \boldsymbol{\zeta}$ both lie in regions such that no particle center lies within a radius $x$ of point $\mathbf{r}$ or within a radius $y$ of point $\mathbf{r} + \boldsymbol{\zeta}$. Define $\Omega_x$ and $\Omega_y$ to be these spherical regions surrounding points $\mathbf{r}$ and $\mathbf{r} + \boldsymbol{\zeta}$, respectively, and define $\Omega$ to be the total region $\Omega = \Omega_x \cup \Omega_y$. If we restrict $x$ and $y$ so that $x, y \leqslant R$, then $\Omega$ can be occupied by zero, one, or at most two particle centers. In the isotropic case, the probability that $\Omega$ is empty takes the form

$$H(\zeta; x, y) = 1 - V_\Omega(\zeta; x, y) + \frac{1}{2}\rho^2 \int_\Omega \int_\Omega g(|\mathbf{r}' - \mathbf{r}''|)\, d^3r'\, d^3r''. \tag{16}$$

The volume of the region $\Omega$ is $V_\Omega(\zeta; x, y)$ and is given by

$$\begin{aligned}
V_\Omega(\zeta; x, y) &= \frac{4\pi}{3} x^3 \qquad \text{for} \quad x > y \\
&\qquad\qquad\qquad\qquad\qquad\qquad\qquad\qquad\qquad\qquad \zeta < |x - y| \\
&= \frac{4\pi}{3} y^3 \qquad \text{for} \quad y > x \\
&= \frac{\pi}{6}(x + y + \zeta)^3 \qquad\qquad\qquad\qquad\qquad\qquad \zeta = |x - y| \qquad (17) \\
&= \pi(x + y + \zeta)^2 \left[\frac{(x - y)^2}{4\zeta} + \frac{1}{6}\left(x + y - \frac{\zeta}{2}\right)\right] \qquad |x - y| < \zeta \leqslant x + y \\
&= \frac{4\pi}{3}(x^3 + y^3) \qquad\qquad\qquad\qquad\qquad\qquad \zeta > x + y.
\end{aligned}$$

Equation (16) can be simplified slightly. Since the radial distribution function vanishes for $|\mathbf{r} - \mathbf{r}'| < \sigma$ and since we have restricted $x$ and $y$ to be less than or equal to $R = \sigma/2$, we see that

$$\frac{1}{2}\int_\Omega \int_\Omega g(|\mathbf{r}' - \mathbf{r}''|)\, d^3r'\, d^3r'' = \int_{\Omega_x} \int_{\Omega_y} g(|\mathbf{r}' - \mathbf{r}''|)\, d^3r'\, d^3r''. \tag{18}$$

Combining (16)–(18) and substituting into (13)–(15), we find first that the void–void correlation function is given by

$$F_{vv}(\zeta) = 1 - \rho V_\Omega(\zeta; R, R) + \rho^2 I_{vv}(\zeta) \tag{19}$$

where

$$V_\Omega(\zeta; R, R) = \frac{4\pi}{3} R^3 \left[1 + \frac{3\zeta}{4R}\left(1 - \frac{\zeta^2}{12R^2}\right)\right] \qquad \zeta \leqslant 2R$$
$$= \frac{8\pi}{3} R^3 \qquad \zeta > 2R \tag{20}$$

and

$$I_{vv}(\zeta) = \int_{\Omega_R}\int_{\Omega_R} g(|\zeta\hat{z} + \mathbf{r}'' - \mathbf{r}'|)\, d^3r'\, d^3r''. \tag{21}$$

The region $\Omega_R$ is a spherical region of radius $R$ centered at the origin. We have used the isotropy of $g$ in reducing (18) to (21). Similarly, the surface–void correlation function is

$$F_{sv}(\zeta) = \rho \left.\frac{\partial V_\Omega(\zeta; x, y)}{\partial x}\right|_{x=y=R} - \rho^2 I_{sv}(\zeta) \tag{22}$$

where

$$\left.\frac{\partial V_\Omega(\zeta; x, y)}{\partial x}\right|_{x=y=R} = 2\pi R^2(1 + \zeta/2R) \qquad \zeta \leqslant 2R$$
$$= 4\pi R^2 \qquad \zeta > 2R \tag{23}$$

and

$$I_{sv}(\zeta) = R^2 \int_{S_R}\int_{\Omega_R} g(|\zeta\hat{z} + R\hat{r}(\theta'', \phi'') - \mathbf{r}'|)\, d^3r' \sin\theta''\, d\theta''\, d\phi'' \tag{24}$$

and furthermore the surface–surface correlation function is

$$F_{ss}(\zeta) = -\rho \left.\frac{\partial^2 V_\Omega(\zeta; x, y)}{\partial x\, \partial y}\right|_{x=y=R} + \rho^2 I_{ss}(\zeta) \tag{25}$$

where

$$\left.\frac{\partial^2 V_\Omega}{\partial x\, \partial y}\right|_{x=y=R} = -\frac{2\pi R^2}{\zeta} \qquad 0 < \zeta \leqslant 2R$$
$$= 0 \qquad \zeta > 2R \tag{26}$$

and

$$I_{ss}(\zeta) = R^4 \int_{S_R}\int_{S_R} g(|\zeta\hat{z} + R\hat{r}(\theta'', \phi'') - R\hat{r}(\theta', \phi')|$$
$$\times \sin\theta'\, d\theta'\, d\phi'\, \sin\theta''\, d\theta''\, d\phi''. \tag{27}$$

In Eqs. (24) and (27), $S_R$ is the surface of the sphere of radius $R$ centered at the origin.

To check that the limiting forms of (19), (22), and (25) are correct as $\zeta \to \infty$, note that

$$F_{vv}(\zeta) \to 1 - \frac{8\pi}{3} R^3 \rho + \left(\frac{4\pi}{3} R^3\right)^2 \rho^2 = \phi^2 \tag{28}$$

$$F_{sv}(\zeta) \to 4\pi R^2 \rho - (4\pi R^2)\left(\frac{4\pi}{3} R^3\right) \rho^2 = s\phi \tag{29}$$

$$F_{ss}(\zeta) \to 0 + (4\pi R^2)^2 \rho^2 = s^2 \tag{30}$$

since $g \to 1$ as $\zeta \to \infty$, $\phi = 1 - \eta$, and $s = 4\pi R^2 \rho$. Equation (19) is the same as Eq. (6) of Weissberg and Prager [21] except for an apparent typographical error in [21]. Furthermore, Eq. (19) also yields (8) as $\zeta \to 0$ after some tedious manipulations which will not be reproduced here.

The final computation of the bounds (2) and (3) now reduces to the numerical problem of evaluating the multidimensional integrals appearing in (21), (24), and (27). Even for the simplest non-trivial choice of radial distribution function, these integrals are quite tedious to evaluate. Section 3 presents an analytical example using the well-stirred approximation. Section 4 presents more realistic calculations based on radial distribution functions valid for higher packing fractions. Such calculations necessarily require Monte Carlo integration.

## 3. Analytical Example: Well-Stirred Approximation

The simplest non-trivial approximation to the hard-sphere radial distribution function is based on the assumption that, except for the hard-sphere excluded volume, particle locations are uncorrelated. The corresponding radial distribution function is

$$\begin{aligned} g_{ws}(r) &= 0 \qquad \text{for} \quad r < \sigma \\ &= 1 \qquad \text{for} \quad r \geqslant \sigma. \end{aligned} \tag{31}$$

This approximation to $g(r)$ is sometimes known as the well-stirred approximation [22]. This approximation becomes exact for all $r$ as the number density $\rho \to 0$. It is also a good approximation to $g(r)$ for all $\rho$ as $r \to \infty$. It is nevertheless a very unrealistic radial distribution function as we will soon show. However, by using (31), we can evaluate (21), (24), and (27) analytically. This calculation serves three important functions: (1) It provides insight into the difficulties inherent in evaluating these multidimensional integrals. (2) It provides exact results which can be used to check the accuracy of our Monte Carlo integration routine. (3) The resulting formulas often aid us in reducing the number of iterations required by our Monte

Carlo integrations while still achieving the desired degree of accuracy. Since the integrals are linear in $g(r)$ and since we can write in general

$$g(r) = g_{ws}(r) + \Delta g(r) \tag{32}$$

where $\Delta g$ vanishes identically for $r < \sigma$ and is negligible for large $r$ ($\geqslant 5\sigma$), a significant contribution to the correlation functions for $\zeta$ comes from (31). In general, the integrals of interest have the form

$$I(\zeta) = I_{ws}(\zeta) + \Delta I(\zeta) \tag{33}$$

where $\Delta I/I_{ws}$ is often (but not always) quite small.

To calculate (21), we will first write down a transformed version of the integral and then motivate the transformations. First, the integral is rewritten as

$$I_{vv}(\zeta) = \left(\frac{4\pi}{3} R^3\right)^2 - \iint (1 - g_{ws})\, d^3r'\, d^3r'' \tag{34}$$

which can then be evaluated as

$$I_{vv}(\zeta) = \left(\frac{4\pi}{3} R^3\right)^2 - \frac{\pi}{\zeta} \int_{\zeta - R}^{\min(\zeta + R, 3R)} dr\, r[R^2 - (r - \zeta)^2]\, d_{vv}(r)$$

$$\text{for} \quad \zeta \geqslant 2R \tag{35}$$

and

$$\begin{aligned} I_{vv}(\zeta) = {} & \left(\frac{4\pi}{3} R^3\right)^2 - \frac{8\pi^2}{9} R^3 \left(R - \frac{\zeta}{2}\right)^2 \left(2R + \frac{\zeta}{2}\right) \\ & - \frac{\pi^2}{24\zeta} [-54R^4(R^2 - \zeta^2)r + \{72R^3(R^2 - \zeta^2) - 54R^2\zeta\} r^2 \\ & - 2R^2(R^2 - 10\zeta^2 - 48R\zeta) r^3 \\ & - 6R^2(5\zeta + 6R) r^4 + \frac{2}{5}(31R^2 - \zeta^2) r^5 \\ & + \frac{2}{3}\zeta r^6 - \frac{2}{7} r^7 \Big]_R^{\zeta + R} \qquad \text{for} \quad 0 \leqslant \zeta \leqslant 2R. \end{aligned} \tag{36}$$

In (35), the function $d_{vv}(r)$ is given by

$$\begin{aligned} d_{vv}(r) &= \frac{4\pi}{3} R^3 && 0 < r \leqslant R \\ &= \frac{\pi}{3} [h_1^2(3R - h_1) + h_2^2(6R - h_2)] && R \leqslant r \leqslant 3R \\ &= 0 && 3R \leqslant r \end{aligned} \tag{37}$$

and

$$h_1(r) = \frac{4R^2 - (R-r)^2}{2r}, \qquad h_2(r) = \frac{R^2 - (2R-r)^2}{2r}. \tag{38}$$

These formulas are obtained through the arguments which follow. However, before starting this discussion, note that the limiting cases of the integral are $I_{vv} \to 0$ as $\zeta \to 0$ and $I_{vv} \to [(4\pi/3)R^3]^2$ as $\zeta \to 4R$. Also, the significance of (37) and (38) will become clear in our subsequent discussion if we recall that the volume of a spherical segment of height $h$ for a sphere of radius $R_0$ is $(\pi/3)h^2(3R_0 - h)$.

We first consider the case $\zeta \geqslant 2R$. If we make a change of variables from $r''$, $\theta''$ to $r$, $\theta$ as shown in Fig. 1, we find that the relevant overlapping volume (shaded in the figure) depends on $r$ but is independent of $\theta$ and $\phi''$. The volume of this overlap region is the sum of two spherical segments for spheres of radii $R$ and $2R$ whose centers are a distance $r$ apart. This volume is given by $d_{vv}(r)$ in (37). The Jacobian of the transformation is $r/r''$. Integrating with respect to $\theta$ from $\theta = 0$ to $\theta = \theta_{max}$ (at the surface of the sphere) gives a factor

$$(1 - \cos\theta_{max}) = \frac{R^2 - (r-\zeta)^2}{2r\zeta}. \tag{39}$$

Integrating with respect to $\phi''$ gives an additional factor of $2\pi$ which when combined with (39) finally gives (35).

Next consider the case $\zeta < 2R$. The same change of variables used in the preceding paragraph is still useful, but only for $R \leqslant r \leqslant \zeta + R$. For $r < R$, $r$ lies in the region of volume

$$\frac{2\pi}{3}\left(R - \frac{\zeta}{2}\right)^2\left(2R + \frac{\zeta}{2}\right) \tag{40}$$

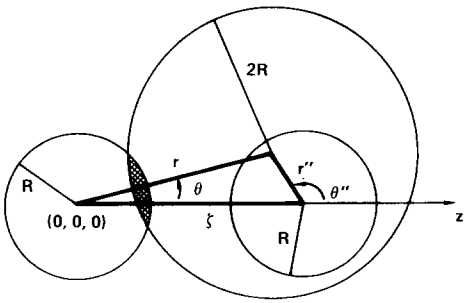


FIG. 1. Illustration of the geometry used in evaluating integrals (21), (24), and (27) when $\zeta \geqslant 2R$. The shaded region of overlap has the volume given in Eq. (37). The surface area of this shaded region is given in Eq. (43).

where the two spheres of radius $R$ overlap (shaded region of Fig. 2). For *every point* in this volume, the entire volume of the sphere at the origin lies within the sphere of radius $2R$. So (40) is multiplied by $4\pi R^3/3$ to obtain the second contribution to (36). The bracketed polynomial constituting the final term in (36) is obtained by replacing the limits of integration in (35) [i.e., $\zeta - R$ and $\min(\zeta + R, 3R)$] by those appropriate for the case $0 \leqslant \zeta \leqslant 2R$ (i.e., $R$ and $\zeta + R$) and then integrating. This concludes the derivation of (35)–(38).

Arguments along similar lines show that the surface–void integral (24) is

$$I_{sv}(\zeta) = \frac{16\pi^2}{3} R^5 - \frac{\pi}{\zeta} \int_{\zeta - R}^{\min(\zeta + R, 3R)} dr\, r[R^2 - (r - \zeta)^2]\, d_{sv}(r) \qquad \text{for} \quad \zeta \geqslant 2R \tag{41}$$

and

$$\begin{aligned} I_{sv}(\zeta) = {} & \frac{16\pi^2}{3} R^5 - \frac{8\pi^2}{3} R^2 \left(R - \frac{\zeta}{2}\right)^2 \left(2R + \frac{\zeta}{2}\right) \\ & - \frac{\pi^2}{\zeta} R \left[3R^2(R^2 - \zeta^2) r + R(R^2 + 3R\zeta - \zeta^2) r^2 \right. \\ & \left. + \frac{1}{3}(\zeta^2 + 4R\zeta - 4R^2) r^3 - \frac{1}{2}(R + \zeta) r^4 + \frac{1}{5} r^5 \right]_R^{\zeta + R} \qquad \text{for} \quad \zeta < 2R \end{aligned} \tag{42}$$

where

$$\begin{aligned} d_{sv}(r) &= 4\pi R^2 && 0 < r \leqslant R \\ &= 2\pi R h_1(r) && R \leqslant r \leqslant 3R \\ &= 0 && 3R \leqslant r \end{aligned} \tag{43}$$

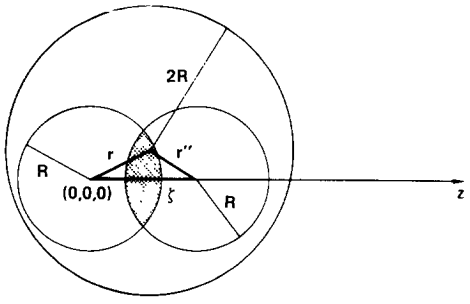


FIG. 2. Illustration of the geometry used in evaluating integrals (21), (24), and (27) when $\zeta < 2R$. The shaded region of overlap has the volume given in Eq. (40).

and $h_1(r)$ is given by (38). Similarly, the surface–surface integral (27) is given by

$$I_{ss}(\zeta) = (4\pi R^2)^2 - \frac{2\pi^2 R^2}{\zeta} \int_{\zeta - R}^{\min(\zeta + R, 3R)} dr |4R^2 - (R - r)^2| \qquad \text{for} \quad 2R \leqslant \zeta \leqslant 4R \tag{44}$$

and

$$I_{ss}(\zeta) = (4\pi R^2)^2 - 8\pi^2 R^3 \left(R - \frac{\zeta}{2}\right) - \frac{2\pi^2 R^2}{\zeta} \left[3R^2 r + Rr^2 - \frac{1}{3} r^3\right]_R^{\zeta + R} \qquad \text{for} \quad \zeta < 2R. \tag{45}$$

Even in this relatively simple case, we see that the required manipulations are quite tedious. When more realistic radial distribution functions are used, numerical methods are necessarily required. Furthermore, since the domain of integration is so complex and since the integrand is so poorly behaved (vanishing identically for $|\mathbf{r}' - \mathbf{r}''| > 2R$), it follows that an accurate, adaptive multidimensional Monte Carlo integration scheme is needed. The method which we have used with success is the routine VEGAS by Lepage [14]. This routine uses importance sampling to alter the grid and also possesses a natural estimate of the accuracy of the final result based on the variance per iteration. Both of these characteristics are essential in the present application.

To check the accuracy of the Monte Carlo integration routine (and incidentally to check our arithmetic in the analytical solution), we have calculated the integrals $I_{vv}$, $I_{sv}$, and $I_{ss}$ numerically using VEGAS. The maximum number of iterations was set equal to 10. The other parameters in VEGAS (see Lepage [14]) are $N = 50$ (storage locations) and $\alpha = 1.5$ (exponent for damping the subdivision algorithm). Iterations were terminated prior to the 10th iteration if the estimated variance was less than 2 %. Two cases were run. The number of function evaluations per iteration was less than 3000 in the first case and less than 8200 in the second case. (VEGAS chooses the precise number of function evaluations depending on the allowed maximum.)

The results for $\sigma = 2R = 1$ are presented in Table I. In the columns labelled "VEGAS," the first number for given $\zeta/\sigma$ is the result for less than 3000 function evaluations and the second number for less than 8200 function evaluations. Numbers in parentheses are results after 10 iterations for which the algorithm's estimated accuracy failed to achieve the requested value of 2%. The actual number of total iterations required depended on both $\zeta$ and the particular integral being evaluated. In the first case, the successful integration of $I_{vv}(\zeta)$ required a maximum of six iterations for $\zeta/\sigma = 0.1$ and two iterations or less for $\zeta/\sigma \geqslant 0.4$. In the second case, the number of iterations for a successful integration was generally two or three times smaller for the smaller values of $\zeta$ while two iterations or less were required for $\zeta/\sigma > 0.4$. Clearly, the algorithm has no chance to adapt if the integration terminates after only one iteration.

TABLE I

Comparison of the Exact and Monte Carlo (VEGAS) Results for Integrals (21), (24), and (27) Evaluated Using the Well-Stirred Approximation (31) for the Radial Distribution Function

| | $I_{vv}(\zeta)$ | | $I_{sv}(\zeta)$ | | $I_{ss}(\zeta)$ | |
|---|---|---|---|---|---|---|
| $\zeta/\sigma$ | EXACT | VEGAS | EXACT | VEGAS | EXACT | VEGAS |
| 0.10 | 3.866E−04 | (2.373E−04) | 1.602E−02 | (1.333E−0.3) | 5.099E−01 | 5.025E−01 |
| | | (3.527E−04) | | 1.412E−02 | | 4.987E−01 |
| 0.20 | 2.896E−03 | (2.477E−03) | 6.224E−02 | 5.507E−02 | 1.053E+00 | 1.041E+00 |
| | | 2.742E−03 | | 6.105E−02 | | 1.037E+00 |
| 0.40 | 2.003E−02 | 1.990E−02 | 2.327E−01 | 2.292E−01 | 2.237E+00 | 2.263E+00 |
| | | 1.894E−02 | | 2.319E−01 | | 2.270E+00 |
| 0.60 | 5.721E−02 | 5.722E−02 | 4.820E−01 | 4.812E−01 | 3.553E+00 | 3.524E+00 |
| | | 5.701E−02 | | 4.806E−01 | | 3.509E+00 |
| | | 1.118E−01 | | 7.683E−01 | | 5.062E+00 |
| 1.00 | 1.723E−01 | 1.726E−01 | 1.069E+00 | 1.079E+00 | 6.580E+00 | 6.511E+00 |
| | | 1.734E−01 | | 1.050E+00 | | 6.601E+00 |
| 1.20 | 2.235E−01 | 2.250E−01 | 1.305E+00 | 1.395E+00 | 7.940E+00 | 7.998E+00 |
| | | 2.234E−01 | | 1.318E+00 | | 7.935E+00 |
| 1.40 | 2.554E−01 | 2.568E−01 | 1.496E+00 | 1.507E+00 | 8.854E+00 | 8.933E+00 |
| | | 2.529E−01 | | 1.504E+00 | | 8.877E+00 |
| 1.60 | 2.699E−01 | 2.703E−01 | 1.598E+00 | 1.603E+00 | 9.442E+00 | 9.576E+00 |
| | | 2.726E−01 | | 1.586E+00 | | 9.430E+00 |
| 1.80 | 2.739E−01 | 2.711E−01 | 1.639E+00 | 1.617E+00 | 9.767E+00 | 9.715E+00 |
| | | 2.756E−01 | | 1.628E+00 | | 9.765E+00 |
| 2.00 | 2.742E−01 | 2.752E−01 | 1.645E+00 | 1.647E+00 | 9.870E+00 | 9.882E+00 |
| | | 2.721E−01 | | 1.629E+00 | | 9.849E+00 |

*Note.* The two values listed under VEGAS for each choice of $\zeta$ are results for different maximum numbers of function evaluations per iteration: the first value has less than 3000 evaluations per iteration and the second had less than 8200. The maximum number of iterations was 10 and the specified accuracy for a successful integration was 2%. Values in parentheses are final values obtained after 10 iterations when the 2% accuracy criterion was not satisfied.

One interesting detail of the application of this Monte Carlo technique concerns the choice of dimension for the actual integration. First note the azimuthal symmetry of Figs. 1 and 2. It follows that the dimension of each of the three integrals (21), (24), and (27) can be reduced by one since the integrand clearly depends only on the difference $(\phi'' - \phi')$ and not on $\phi', \phi''$ separately. This reduction in dimension was incorporated into an early version of the code. However, it was found that the presence of this additional (redundant) dimension actually helped to improve the results, presumably by increasing the uniformity of the distribution of points picked by the pseudo-random number generator. The results presented in this paper were generated with VEGAS ignoring the azimuthal symmetry.

We conclude from these results that VEGAS works adequately for the present application. We also conclude that it is advantageous to use a larger number of

TABLE II

Computed Drag Coefficients (46) for Prager's Bound ($C_P$) and Doi's Bound ($C_D$) Using the Well-Stirred Approximation for $g(r)$

| | Well-stirred approximation | |
|---|---|---|
| $\eta$ | $C_P$ | $C_D$ |
| 0.000125 | 0.618 | 1.000 |
| 0.0010 | 0.621 | 1.001 |
| 0.06 | 0.866 | 1.076 |
| 0.13 | 1.448 | 1.263 |
| 0.19 | 4.414 | 1.683 |
| 0.25 | ------ | 2.912 |
| 0.32 | ------ | 21.495 |
| 0.38 | ------ | -------- |

*Note.* Dashes indicate values of packing fraction ($\eta$) for which the computed "upper bounds" on permeability become negative—indicating the unrealistic nature of the chosen approximation to the radial distribution function. Note that the limiting value of $C_p$ as $\eta \to 0$ is $C_p = 50/81 = 0.6173$.

function evaluations per iteration for small values of $\zeta/\sigma$ and a smaller number of evaluations for larger values of $\zeta/\sigma$. This philosophy has been employed successfully in the more realistic cases discussed in the next section.

Before concluding this section, we wish to present the bounds on permeability computed using the well-stirred approximation. The results appear in Table II. Except for the first two values of packing fraction, the points chosen are tenths of the random-close-packed density for hard spheres $\eta_{RCP} \simeq 0.64$ [13, 20, 23]. The numbers quoted are the drag coefficients defined by

$$C_P = k_S/k_P \qquad C_D = k_S/k_D \tag{46}$$

where

$$k_S^{-1} = 6\pi\rho R = \frac{9\eta}{2R^2} \tag{47}$$

is the exact result for Stokes flow through a very dilute assemblage of spheres ($\eta \ll 1$), each sphere having radius $R$. Note that, since $k_P$ and $k_D$ are upper bounds on permeability, $C_P$ and $C_D$ are lower bounds on the true drag coefficient. Dashes occur in Table II at points where the computed "upper bounds" $k_P$ or $k_D$ actually become negative. This absurd behavior is typical of results computed using unrealistic radial distribution functions and should not be construed as indicating a failure of the variational methods. These results demonstrate the necessity of using accurate values for $g(r)$ when computing bounds and, therefore, provide an additional motivation for the work discussed in Section 4.

## 4. Numerical Results for Large Packing Fractions

In this section, we discuss the numerical methods used and the results obtained for two models of the hard-sphere radial distribution function. These two models are: (1) the Percus–Yevick (PY) approximation to the hard-sphere $g(r)$ as computed using the exact solution given by Wertheim [15] and Thiele [16] and (2) the semi-empirical approximation to $g(r)$ due to Verlet and Weis [11]. The Verlet–Weis (VW) approximation is obtained by shifting $g_{PY}(r)$ so oscillations in $g_{VW}(r)$ at large $r$ are in phase with results of computer experiments and then adding a short-range correction term near the core ($r = \sigma$) so that $g_{VW}(\sigma)$ agrees with the Carnahan–Starling equation of state [24]. Verlet and Weis state that their radial distribution function differs from the "exact" one in the range $0.35 \leqslant \eta \leqslant 0.49$ by at most 3% and the statistical error is estimated to be about 1%. A computer code for calculating $g_{VW}(r)$ for $r$ up to $r = 5\sigma$ has also been published [17].

A third possibility—that of using the Monte Carlo results directly in tabular form—was rejected on the grounds that the required Monte Carlo integration scheme already limits the accuracy of our results to about 2% (for reasonable total computing time). Thus, the extra effort involved is not warranted.

The numerical method used was the same one described in the preceding section with the following modifications. We take advantage of the observation (32) that $g(r)$ can be split into two parts. The first part is $g_{ws}(r)$ whose analytical contributions to the relevant integrals were calculated in Section 3. The remainder $\Delta g(r)$ vanishes for $r < \sigma$, is negligible for $r > 5\sigma$, and is often quite small in the region $\sigma \leqslant r \leqslant 5\sigma$. The contribution $\Delta I$ due to $\Delta g$ must be computed using Monte Carlo integration; however, the relative error in $I$ is now $\sigma_{\Delta I}/(I_{ws} + \Delta I)$ where $I_{ws}$ is known exactly and $\Delta I/I_{ws}$ becomes quite small as $\zeta \to 6\sigma$. (Both nontrivial models for $g(r)$ approach $g_{ws}(r)$ as $r \to 5\sigma$ so all three computed correlation functions reach their asymptotic values at $\zeta = 6\sigma$.) The major errors in the Monte Carlo integrations occur for small $\zeta$, but Eqs. (2) and (3) both contain a factor of $\zeta$ in the integrand which helps to minimize the effects of these errors in our final results for the variational bounds. For large $\eta$, we have typically set the maximum number of function evaluations per iteration equal to 8200 [number of grid increments per axis in 6-D is $N = (8200/2)^{1/6} = 4$] for small $\zeta$ and reduced this number of 3000 [$N = (1500)^{1/6} = 3$] for larger $\zeta$, e.g., $\sigma \leqslant \zeta \leqslant 6\sigma$.

Computations are conveniently limited to the range $0 < \zeta < 6\sigma$ beyond which the correlation functions take on their asymptotic values (28)–(30). We found that dividing this interval into 60 equal subintervals and then computing the correlation functions at the 59 points of separation gave sufficiently good statistics for the final integrations in (2) and (3). For example, the final integrations are typically of the form

$$\Delta I = \int_0^6 d\zeta\, \zeta F(\zeta) = 0.01 \sum_{n=1}^{59} nF(0.1n) \tag{48}$$

using the trapezoidal rule to evaluate the integral and noting that $F(6) = 0$. Since

$F(0.1n)$ is a random variable with variance $\sigma_n$ estimated by VEGAS, the final integral has an estimated variance of

$$\sigma_{\Delta I}^2 = \sum_{n=1}^{59} (0.01n)^2 \sigma_n^2 \lesssim 7.2\sigma_{\max}^2 \tag{49}$$

with a probable error of

$$0.67\sigma_{\Delta I} \lesssim 1.8\sigma_{\max}. \tag{50}$$

These estimates place upper bounds on the error in the computed integrals of 5–6% if $\sigma_{\max}$ is chosen to be 2%. However, these estimates are generally too pessimistic for two reasons: (1) The main contributions to the total variance $\sigma_{\Delta I}$ come from the $\sigma_n$'s for large $n$, but these $\sigma_n$'s are generally much smaller than $\sigma_{\max}$ since these integrals are easier to compute. (2) These formulas give estimates for the variance in that part of the correlation function integral which must be computed using Monte Carlo methods. However, the complete correlation function contains substantial parts which are known analytically (see Section 3) so (49) and (50) are clearly too large.

On the other hand, the contributions to the sum in (48) do not all have the same sign. In fact, the upper bounds tend to vanish as the packing fraction increases so it

TABLE III

Comparison of Drag coefficients for Prager's Bound ($C_P$) and Doi's Bound ($C_D$) Computed Using the Percus–Yevick Approximation and the Veret–Weiss Semi-empirical Formula for $g(r)$ as the Packing Fraction ($\eta$) Varies

| | Percus–Yevick | | Verlet–Weis | | Kozeny–Carman | Brinkman |
|---|---|---|---|---|---|---|
| $\eta$ | $C_P$ | $C_D$ | $C_P$ | $C_D$ | $C_{KC}$ | $C_B$ |
| 0.000125 | 0.623 | 1.000 | 0.623 | 1.000 | — | 1.024 |
| 0.001 | 0.625 | 1.000 | 0.625 | 1.000 | — | 1.071 |
| 0.06 | 0.83 | 1.00 | 0.83 | 1.00 | — | 1.9 |
| 0.13 | 1.10 | 1.00 | 1.09 | 1.00 | — | 2.8 |
| 0.19 | 1.47 | 1.01 | 1.45 | 1.01 | 3.6 | 4.0 |
| 0.25 | 1.96 | 1.04 | 1.95 | 1.03 | 6.2 | 5.8 |
| 0.32 | 2.59 | 1.09 | 2.64 | 1.10 | 10.1 | 8.7 |
| 0.38 | 3.84 | 1.20 | 3.72 | 1.20 | 16.2 | 11.5 |
| 0.45 | 4.42 | 1.27 | 4.39 | 1.31 | 26.2 | 23.9 |
| 0.49 | 4.65 | 1.35 | 4.58 | 1.37 | 36.9 | 38.6 |
| | | | Finney | | | |
| 0.64 | — | — | 7.42 | — | 133 | — |

*Note.* Also shown are results for the Kozeny–Carman relation (51) and Brinkman's mean field theory (52). The value for $\eta = 0.64$ was obtained using unpublished values of the radial distribution function for a laboratory packing of spheres, courtesy of J. L. Finney [13, 27].

becomes quite difficult to make *a priori* estimates of the accuracy of our results at high $\eta$. This uncertainty can be resolved by numerical checks.

For example, numerical tests done by computing the bounds for different values of VEGAS input parameters show that the results in Table III change by less than 2% as the chosen $\sigma_{max}$ in VEGAS decreases and the number of grid points for Eqs. (2) and (3) increases. Hence, the results for the PY model are expected to be correct for that model within about 2%. If we consider the VW results to represent estimates of results which would be obtained using Monte Carlo $g(r)$'s directly, the expected error of the VW values in Table III is certainly less than 5% and probably about 2–3%. However, we have not checked for possible systematic discrepancies between $g_{VW}(r)$ and the Monte Carlo results which might alter this conclusion.

The results for the bounds on drag coefficients are presented in Table III and plots of normalized bounds on permeability are presented in Figs. 3 and 4. For comparison, the empirical correlation due to Kozeny and Carman

$$C_{KC} \approx 10\eta/(1-\eta)^3 \tag{51}$$

and the theoretical (effective medium) estimate of permeability due to Brinkman

$$C_B^{-1} = 1 + \frac{3\eta}{4}\left[1 - (8/\eta - 3)^{1/2}\right] \tag{52}$$

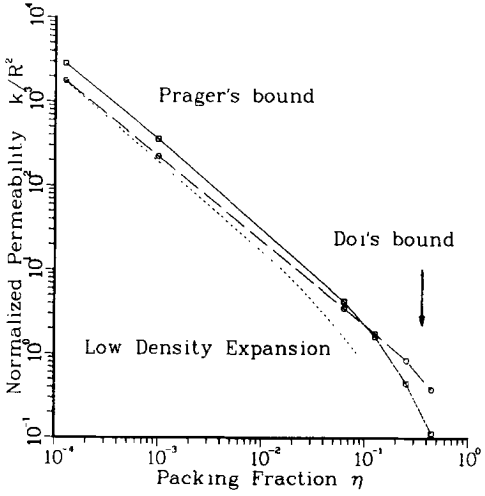


FIG. 3. Comparison of Prager's bound (boxes and solid line) and Doi's bound (circles and dot-dash line) for the normalized permeability $k/R^2$ for random aggregates of spheres using the Verlet–Weis semi-empirical formula for $g(r)$. This plot illustrates the behavior at asymptotically low values of packing fraction $\eta$. The exact asymptotic result (53) is shown with a dashed line.

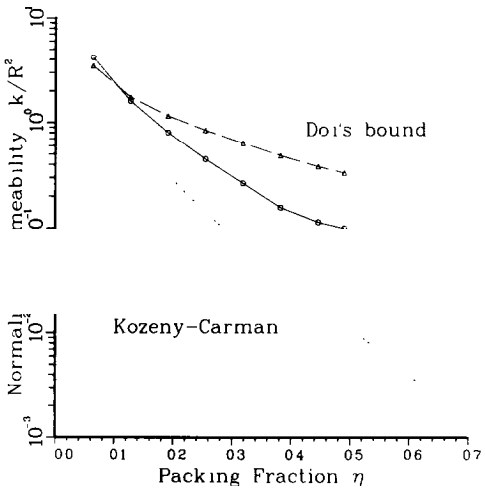


FIG. 4. Comparison of Prager's bound (circles, box, and solid line) and Doi's bound (triangles and dot-dash line) for the normalized permeability $k/R^2$ for random aggregates of spheres. This plot illustrates the behavior at large values of packing fraction $\eta$. The values at circles and triangles were computed using the Verlet–Weis semi-empirical formula for $g(r)$. The value for the box point at $\eta = 0.64$ was computed using Finney's empirical radial distribution function for a laboratory packing of spheres [13, 27]. The Kozeny–Carman empirical relation (51) is shown with a dashed line.

is also presented [25]. The asymptotic estimate for small values of $\eta$ which was obtained in the work of Childress [3], Howells [4], and Hinch [5] is given by

$$C_A = 1 + \frac{3}{\sqrt{2}}\eta^{1/2} + \frac{135}{64}\eta \ln \eta + 16.5\eta + \cdots \tag{53}$$

and is plotted in Fig. 3. The experimental values for aggregates of spheres are known not to differ much from the Kozeny–Carman empirical correlation [26].

Various features of the results in Table III require discussion. First, note that Doi's bound is better than Prager's bound for packing fractions less than about 10% and vice versa for packing fractions greater than 10%. Next, note that, for either choice of radial distribution function, both lower bounds on the drag coefficients $C$ increase monotonically up to $\eta = 0.49$. For $\eta > 0.49$, neither radial distribution function is reliable. For example, the Percus–Yevick radial distribution function is known to have (unphysical) negative values in some regions for higher values of $\eta$. Attempts to compute the bounds for higher values of $\eta$ have been made but we found the results to be of no use. The computed "bounds" are not necessarily monotonic in the region $0.49 < \eta < 0.64$ and were observed to be negative for certain values of $\eta$, again indicating the unrealistic nature of these radial distribution functions where extrapolated outside their accepted region of validity. Since the case of $\eta = \eta_{RCP} \simeq 0.64$ is of special interest—corresponding to the random aggregate of spheres most likely to simulate realistic granular materials—we have obtained the

actual values for $g(r)$ measured for a laboratory sphere packing from Finney [27] and used this histogram to calculate the final value of $C_P$ in Table III. [We also did the same analysis using the $g(r)$ obtained from Bennett's computer-generated sphere packing [12]; however, the resulting bound ($C_P = 0.54$) for $\eta = 0.62$ is so poor that we choose not to quote it in Table III.] At random close packing, the radial distribution function has a delta function singularity at $r = \sigma$ which has been integrated analytically in the Appendix. Since the contributions $\delta I_{sv}$ and $\delta I_{ss}$ turn out to be elliptic integrals and since Doi's bound is so much worse than Prager's for large $\eta$, we have chosen not to evaluate $C_D$ for $\eta = 0.64$.

We expect the Verlet–Weis approximation for $g(r)$ to be more accurate than the Percus–Yevick approximation for the larger values of $\eta$. Nevertheless, we find that the results for the variational bounds do not depend strongly on which of these two choices we make.

Figure 3 shows that Doi's bound approaches the correct asymptotic limit as $\eta \to 0$ while Prager's bound does not. Figure 4 shows that Prager's bound is closer to observed values of permeability than Doi's bound is for larger values of $\eta$. However, even Prager's bound differs from measured values by a factor of 5 at $\eta \sim 0.40$ and by more than an order of magnitude at $\eta = 0.64$. The results are disappointing from this point of view. On the other hand, Prager [9] has also published variational bounds depending on three-point correlation functions which will necessarily be better estimates of the empirical values than those obtained here using only two-point correlation functions. The present work may therefore be viewed as an essential prerequisite to the evaluation of these are more complicated variational bounds.

## 5. Summary and Conclusions

In this paper, we have presented the numerical methods required to evaluate the variational bounds derived by Prager [9] and Doi [10] for fluid permeability in the case of random aggregates of spheres. We find that Doi's bounds are close to the exact results for small packing fractions but that Prager's bounds are superior to Doi's for large packing fractions. The results for both bounds are disappointingly far from the experimental values at the larger packing fractions. This quantitative failure of the bounds may be due to the restriction to two-point correlation functions or it may be more general. Presumably bounds using three-point correlation functions (such as those of Prager [9]) will provide improved estimates of the permeability for higher values of $\eta$. However, three-point (or higher multi-point) correlation functions are not as yet known with nearly as much accuracy as the two-point correlation functions [29]. Detailed calculations using bounds with three-point correlation functions must for now remain a task for future research.

## APPENDIX

For aggregates of spheres in the random-close-packing limit ($\eta_{RCP} \sim 0.64$), the radial distribution function exhibits a new feature not present for smaller values of packing fraction. Bennett [12] has pointed out the existence of a delta function singularity in $g(r)$ located at $r = \sigma$, the diameter of the spheres. This delta function arises because the cumulative radial distribution function

$$G(r) = 4\pi\rho \int_0^r g(\lambda)\, \lambda^2\, d\lambda \tag{A1}$$

has a step discontinuity at $r = \sigma$ since $G(r) = 0$ for $r < \sigma$ and $G(\sigma) \neq 0$. In fact, $G(\sigma)$ is just the coordination number (the average number of spheres touching each sphere) in the random-close-packing limit. It follows that $g(r)$ can be written as

$$g(r) = \frac{G(\sigma)}{4\pi\sigma^2\rho}\, \delta(r - \sigma) + \text{continuous part.} \tag{A2}$$

The value of $G(\sigma)$ is generally thought to be $G(\sigma) = 6$ for random close packing in three dimensions [12, 28] based on stability arguments. Furthermore, $G(\sigma) = 6$ is consistent [27] with Finney's experimental data [13]. We will assume $G(\sigma) = 6$ exactly in this paper.

The delta function contribution to the integrals (21), (24), and (27) can be evaluated analytically. It is also easy to see that the integration follows nearly the same lines as those presented in Section 3 for the well-stirred approximation. The principal difference in the analysis for $I_{vv}(\zeta)$ is that, instead of inserting the appropriate *volume* $d_{vv}(r)$ of spherical segments for the region of intersection in Fig. 1, we require a *surface area* of intersection where the spherical surface of radius $2R$ intersects the volume of the sphere of radius $R$. The surface area of a spherical segment is $2\pi R_0 h$ so we find easily that the contribution to $I_{vv}(\zeta)$ from the delta function in $g(r)$ is

$$\delta I_{vv}(\zeta) = \frac{3}{8R^2\rho\zeta} \int_{\zeta - R}^{\zeta + R} dr\, r[R^2 - (r - \zeta)^2]\, e_{vv}(r) \qquad \text{for} \quad 0 \leqslant \zeta \leqslant 4R \tag{A3}$$

where

$$\begin{aligned} e_{vv}(r) &= 4\pi R h_2(r) \qquad R \leqslant r \leqslant 3R \\ &= 0 \qquad\qquad\quad \text{otherwise} \end{aligned} \tag{A4}$$

and $h_2(r)$ is given by (38). Equation (A3) can be integrated to yield

$$\delta I_{vv}(\zeta) = \frac{3\pi}{4R\rho\zeta}\left[R^4 r + \frac{1}{3}(\zeta - 2R)^2 (r-\zeta)^3 - \frac{1}{3}R^2(r-\zeta)^3 - \frac{1}{3}R^2(r-2R)^3 + \frac{1}{5}(r-\zeta)^5\right]_{\max(\zeta-R,R)}^{\min(\zeta+R,3R)}. \tag{A5}$$

The contributions to $I_{sv}(\zeta)$ and $I_{ss}(\zeta)$ arise from the circular intersections of two spherical surfaces and are given by

$$\delta I_{sv}(\zeta) = \frac{3}{8R^2\rho\zeta}\int_{\zeta-R}^{\zeta+R} dr\, r[R^2 - (r-\zeta)^2]\, e_{sv}(r) \qquad \text{for} \quad 0 \leqslant \zeta \leqslant 4R \tag{A6}$$

and

$$\delta I_{ss}(\zeta) = \frac{3}{4R\rho\zeta}\int_{\zeta-R}^{\zeta+R} dr\, r e_{sv}(r) \qquad \text{for} \quad 0 \leqslant \zeta \leqslant 4R \tag{A7}$$

where

$$\begin{aligned} e_{sv}(r) &= \frac{\pi}{r}(9R^2 - r^2)^{1/2}(r^2 - R^2)^{1/2} \qquad R \leqslant r \leqslant 3R \\ &= 0 \qquad\qquad\qquad\qquad\qquad\qquad \text{otherwise.} \end{aligned} \tag{A8}$$

Both expressions (A6) and (A7) reduce to elliptic integrals.

*Note added in proof.* After this paper was accepted for publication, I learned of some relevant work which deserves mention. In his dissertation, Torquato discusses a different numerical method for calculating the correlation functions and then applies his results to the calculation of Prager's bounds on permeability. The results obtained are comparable to the results presented here. This work is being published in a series of papers by Torquato and Stell in *J. Chem. Phys.*

## ACKNOWLEDGMENTS

I wish to thank W. G. Hoover, F. H. Ree, and O. R. Walton for at least a couple of very helpful remarks apiece. I also wish to thank F. N. Fritsch for directing my attention to Ref. [14] and for supplying me with a copy of VEGAS. Work was performed under the auspices of the U.S. Department of Energy by the Lawrence Livermore National Laboratory under Contract W-7405-ENG-48.

## REFERENCES


1. M. J. BERAN, "Statistical Continuum Theories," Chap. 6, Interscience, New York, 1968.
2. H. HASIMOTO, *J. Fluid Mech.* **5** (1959), 317.
3. S. CHILDRESS, *J. Chem. Phys.* **56** (1972), 2527.
4. I. D. HOWELLS, *J. Fluid Mech.* **64** (1974), 449.
5. E. J. HINCH, *J. Fluid Mech.* **83** (1977), 695.
6. A. A. ZICK AND G. M. HOMSY, *J. Fluid Mech.* **115** (1982), 13.
7. A. S. SANGANI AND A. ACRIVOS, *in* "Macroscopic Properties of Disordered Media" (R. Burridge, S. Childress, and G. Papanicolaou, Eds.), pp. 216–225, Lecture Notes in Physics No. 154, Springer-Verlag, Berlin, 1982.
8. J. BEAR, "Dynamics of Fluids in Porous Media," p. 166, American Elsevier, New York, 1975; R. B. BIRD, W. E. STEWART, AND E. N. LIGHTFOOT, "Transport Phenomena," pp. 196–200, Wiley, New York, 1960; T. W. LAMBE AND R. V. WHITMAN, "Soil Mechanics," p. 287, Wiley, New York, 1969.
9. S. PRAGER, *Phys. Fluids* **4** (1961), 1477.
10. M. DOI, *J. Phys. Soc. Japan* **40** (1976), 567.
11. L. VERLET AND J.-J. WEIS, *Phys. Rev. A* **5** (1972), 939.
12. C. H. BENNETT, *J. Appl. Phys.* **43** (1972), 2727.
13. J. L. FINNEY, *Proc. Roy. Soc. London Ser. A* **319** (1970), 479.
14. G. P. LEPAGE, *J. Comput. Phys.* **27** (1978), 192.
15. M. S. WERTHEIM, *Phys. Rev. Lett.* **10** (1963), 321.
16. E. THIELE, *J. Chem. Phys.* **39** (1963), 474.
17. D. HENDERSON, *in* "Statistical Mechanics," by D. A. McQuarrie, Appendix D, pp. 600–603, Harper & Row, New York, 1976.
18. P. B. CORSON, *J. Appl. Phys.* **45** (1974), 3159.
19. J. D. BERNAL, *Proc. Roy. Soc. London Ser. A* **280** (1964), 299.
20. G. D. SCOTT AND D. M. KILGOUR, *J. Phys. D* **2** (1969), 863.
21. H. L. WEISSBERG AND S. PRAGER, *Phys. Fluids* **5** (1962), 1390.
22. G. K. BATCHELOR AND J. T. GREEN, *J. Fluid Mech.* **56** (1972), 401.
23. J. G. BERRYMAN, *Phys. Rev. A* **27** (1983), 1053.
24. N. F. CARNAHAN AND K. E. STARLING, *J. Chem. Phys.* **51** (1969), 635.
25. P. C. CARMAN, "Flow of Gases through Porous Media," Sect. 8.2, Academic Press, New York, 1956.
26. H. RUMPF AND A. R. GUPTE, *Chem. Ing. Tech.* **43** (1971), 367; F. A. L. DULLIEN, "Porous Media-Fluid Transport and Pore Structure," pp. 159–161, Academic Press, New York, 1979.
27. J. L. FINNEY, private communication.
28. K. GOTOH AND J. L. FINNEY, *Nature* **252** (1974), 202.
29. Y. UEHARA, Y.-T. LEE, T. REE AND F. H. REE, *J. Chem. Phys.* **70** (1979), 1884.